JPn Neuroscience

The Journal of Physiology

J Physiol 592.7 (2014) pp 1619–1636

Photoresponse diversity among the five types of intrinsically photosensitive retinal ganglion cells

Xiwu Zhao[1], Ben K. Stafford[1], Ashley L. Godin[3], W. Michael King[3] and Kwoon Y. Wong[1,2]

Departments of [1]Ophthalmology & Visual Sciences, [2]Molecular, Cellular & Developmental Biology and [3]Otolaryngology, University of Michigan, Ann Arbor, MI, USA

Key points

- Intrinsically photosensitive retinal ganglion cells (ipRGCs) are a rare population of retinal output neurons that drives subconscious physiological responses to light, e.g. pupillary constriction, synchronization of daily rhythms to the light–dark cycle and regulation of hormone secretion.
- This study investigated the functional diversity among the five known types of ipRGCs, named M1–M5.
- We found that M2–M5 cells could detect spatial differences in light intensity, implicating an ability to analyse the form of visual stimuli.
- All five ipRGC types responded robustly to moving lights, and M1–M4 cells appeared to respond optimally to different speeds, suggesting they might analyse the speed of motion.
- M1–M4 cells were shown to project to the superior colliculus, a brain area known to detect novel objects in the visual scene, suggesting that the form and motion information signalled by these four types of ipRGCs could contribute to this visual function.

Abstract Intrinsically photosensitive retinal ganglion cells (ipRGCs) mediate non-image-forming visual responses, including pupillary constriction, circadian photoentrainment and suppression of pineal melatonin secretion. Five morphological types of ipRGCs, M1–M5, have been identified in mice. In order to understand their functions better, we studied the photoresponses of all five cell types, by whole-cell recording from fluorescently labelled ipRGCs visualized using multiphoton microscopy. All ipRGC types generated melanopsin-based ('intrinsic') as well as synaptically driven ('extrinsic') light responses. The intrinsic photoresponses of M1 cells were lower threshold, higher amplitude and faster than those of M2–M5. The peak amplitudes of extrinsic light responses differed among the ipRGC types; however, the responses of all cell types had comparable thresholds, kinetics and waveforms, and all cells received rod input. While all five types exhibited inhibitory amacrine-cell and excitatory bipolar-cell inputs from the 'on' channel, M1 and M3 received additional 'off'-channel inhibition, possibly through their 'off'-sublamina dendrites. The M2–M5 ipRGCs had centre–surround-organized receptive fields, implicating a capacity to detect spatial contrast. In contrast, the receptive fields of M1 cells lacked surround antagonism, which might be caused by the surround of the inhibitory input nullifying the surround of the excitatory input. All ipRGCs responded robustly to a wide range of motion speeds, and M1–M4 cells appeared tuned to different speeds, suggesting that they might analyse the speed of motion. Retrograde labelling revealed that M1–M4 cells project to the superior colliculus, suggesting that the contrast and motion information signalled by these cells could be used by this sensorimotor area to detect novel objects and motion in the visual field.

DOI: 10.1113/jphysiol.2013.262782

(Received 27 July 2013; accepted after revision 5 January 2014; first published online 6 January 2014)
Corresponding author K. Y. Wong: Kellogg Eye Center, 1000 Wall Street, Ann Arbor, MI 48105, USA. Email: kwoon@umich.edu

Abbreviations D-AP5, D-(−)-2-amino-5-phosphonopentanoic acid; dLGN, dorsal lateral geniculate nucleus; DNQX, 6,7-dinitroquinoxaline-2,3-dione; DSI, direction selectivity index; $E_{cations}$, reversal potential for cations; E_{Cl}, reversal potential for Cl^-; FITC, fluorescein isothiocyanate; GFP, green fluorescent protein; ipRGC, intrinsically photosensitive retinal ganglion cell; L-AP4, L-(+)-2-amino-4-phosphonobutyric acid; MEA, multielectrode array; OPN, olivary pretectal nucleus; PAG, periaqueductal grey; SC, superior colliculus; SCN, suprachiasmatic nucleus.

Introduction

In the mammalian retina, about 0.2–4% of ganglion cells express the photopigment melanopsin and are directly photoreceptive (Berson *et al.* 2002; Dacey *et al.* 2005; Ecker *et al.* 2010). Five morphological types of these intrinsically photosensitive retinal ganglion cells (ipRGCs), named M1–M5, have been discovered, and they mediate various non-image-forming as well as image-forming visual functions (Hattar *et al.* 2003; Ecker *et al.* 2010; Brown *et al.* 2012). Two methods have been employed to identify these rare cells for electrophysiological characterization. First, to enable targeted whole-cell recording, they have been labelled either by fluorescent tracer dyes injected into the suprachiasmatic nucleus (SCN; Berson *et al.* 2002; Lucas *et al.* 2003; Warren *et al.* 2003) or by genetically encoded fluorescent proteins (Schmidt *et al.* 2008; Do *et al.* 2009; Ecker *et al.* 2010). Second, in multielectrode-array (MEA) recordings, ipRGCs can be distinguished from conventional ganglion cells based on their melanopsin-mediated photosensitivity during synaptic blockade (Tu *et al.* 2005; Wong *et al.* 2007; Weng *et al.* 2013). Previous studies using these methods have yielded important insights into the functional properties and diversity of ipRGCs. For example, the five ipRGC types show diverse ionic currents and current-induced spiking patterns (Schmidt & Kofuji, 2009; Hu *et al.* 2013), and M1 and M2 cells have different resting membrane potentials (Schmidt & Kofuji, 2010). In addition, most if not all ipRGCs generate extrinsic, synaptically driven photoresponses as well as intrinsic light responses (Wong *et al.* 2007), and the sensitivities and kinetics of both responses have been reported to differ among some ipRGC types (Schmidt & Kofuji, 2009, 2010; Ecker *et al.* 2010; Estevez *et al.* 2012). Finally, both the intrinsic and the extrinsic photoresponses of ipRGCs are remarkably tonic, consistent with their role in long-term irradiance coding (Berson *et al.* 2002; Sexton *et al.* 2012; Wong, 2012).

These previous studies had several limitations, however. Specifically, most of the published whole-cell recordings have focused on M1, M2 and M4 cells, and far less is known about M3 and M5. Moreover, nearly all whole-cell-recorded ipRGCs were visualized using intense epifluorescence excitation, which significantly bleached rod/cone photopigments and desensitized melanopsin phototransduction (Wong *et al.* 2005). Consequently, these cells were partly light adapted and gave little information about the behaviour of ipRGCs in dark-adapted conditions. In this respect, MEA recording is a better method because it does not require fluorescence imaging, thereby preserving the dark-adapted state of the retina. However, MEA recording cannot reliably distinguish among the various types of ipRGCs; in fact, it remains unknown whether all five cell types were sampled in previous MEA studies. Furthermore, MEAs cannot be used to assess graded membrane potential changes, and voltage-clamp analysis of ionic currents is impossible.

Here, we have successfully used a multiphoton laser (Wei *et al.* 2010) to target green fluorescent protein (GFP)-labelled ipRGCs for whole-cell recording. One prior study also visualized GFP-labelled ipRGCs in this manner (Viney *et al.* 2007), although the extent to which this approach reduced photobleaching was not assessed, and the only electrophysiological finding was that M2 cells received 'on' amacrine input. In the present study, we first confirmed the effectiveness of this approach in keeping ipRGCs dark adapted and then investigated various aspects of the light-evoked behaviours of all five cell types, including their intrinsic light responses, extrinsic light responses, the contributions of bipolar *vs.* amacrine inputs, receptive field structures and responses to moving stimuli. Finally, through retrograde labelling, we showed that M1–M4 cells project to the superior colliculus (SC), a midbrain nucleus that directs the gaze towards novel stimuli.

Methods

Ethical approval

All experimental procedures were approved by the University Committee on Use and Care of Animals at the University of Michigan.

Animals

A total of ∼400 animals were studied. In the experiment shown in Fig. 4*C*, the animals were *Gnat1*$^{-/-}$ and *Gnat2*^{cpfl3} mice 4–6 months of age. *Gnat1*$^{-/-}$ mice lack the rod transducin α subunit, resulting in non-photosensitive rods (Calvert *et al.* 2000), whereas *Gnat2*^{cpfl3} mice have

a naturally occurring mutation that renders the cone transducin α subunit dysfunctional (Chang *et al.* 2006). All other experiments used mice in which ipRGCs were selectively labelled with GFP. To generate these mice, the *opn4*$^{Cre/Cre}$ line was crossed with a commercially available line in which GFP expression is induced selectively in cells containing Cre, to create *opn4*$^{Cre/+}$*;GFP* animals with one copy of the melanopsin gene (Ecker *et al.* 2010). These *opn4*$^{Cre/+}$*;GFP* mice were between 6 weeks and 3 months of age. All animals were maintained in a 12 h light–12 h dark cycle, and all experiments were performed during the light phase. Mice of both sexes were used.

Electrophysiological recording

Retinal isolation. Prior to each experiment, an animal was dark adapted overnight in a ventilated light-proof box. Under dim red light, the animal was killed using CO_2 inhalation followed by pneumothorax. All subsequent tissue preparation procedures were performed under infrared illumination using night vision devices (NiteMate NAV-3; Litton Industries, Watertown, CT, USA) attached to the eyepieces of a dissecting microscope. Both eyes were harvested, hemisected, and put in room-temperature Ames' medium (Sigma; St Louis, MO, USA) gassed with 95% O_2–5% CO_2. Following vitrectomy using forceps, each retina was isolated from the pigment epithelium and cut into quadrants, which were kept in darkness for up to 7 h prior to recording.

Chemicals and solutions. Two kinds of intracellular solutions were used. For all current-clamp recordings, we used a K^+-based intracellular solution containing (mM): 120 potassium gluconate, 5 NaCl, 4 KCl, 10 Hepes, 2 EGTA, 4 Mg-ATP, 0.3 Na-GTP, 7 Tris-phosphocreatine and either ∼0.1% Lucifer Yellow or ∼0.001% Alexa Fluor568 hydrazide (Life Technologies, Grand Island, NY, USA); and pH was adjusted to 7.3 with KOH. For all voltage-clamp experiments, we used a Cs^+-based intracellular solution containing (mM): 120 caesium methanesulfonate, 3 NaCl, 2 QX-314 chloride, 5 tetraammonium chloride, 10 Hepes, 10 BAPTA tetrapotassium, 2 Mg-ATP, 0.3 Na-GTP and either ∼0.1% Lucifer Yellow or ∼0.001% Alexa Fluor568 hydrazide; and pH was adjusted to 7.3 with NaOH.

The extracellular solution was Ames' medium, which was gassed with 95% O_2–5% CO_2, maintained at 32°C using a temperature controller (Warner Instruments, Hamden, CT, USA), and gravity fed into the superfusion chamber at 2–3 ml min^{-1}. The extracellular solution was recycled using a peristaltic pump. L-(+)-2-Amino-4-phosphonobutyric acid (L-AP4), 6,7-dinitroquinoxaline-2,3-dione (DNQX) and D-(−)-2-amino-5-phosphonopentanoic acid (D-AP5) were purchased from Tocris (Minneapolis, MN, USA). All other chemicals were purchased from Sigma (St Louis, MO, USA) unless noted otherwise.

Whole-cell recording and identification of cell types. Under infrared illumination, a piece of retina was flattened onto a small piece of lens paper on the transparent bottom of a superfusion chamber with the ganglion cell side up, and was held down by a weighted net. The chamber was positioned on a TCS SP5 II confocal microscope (Leica Microsystems, Buffalo Grove, IL, USA) equipped with a Mai Tai DeepSee multiphoton laser (Newport, Irvine, CA, USA), and was shielded from ambient light throughout the experiment. Unless stated otherwise (see the next paragraph), we used a 915 nm multiphoton laser to target GFP-labelled ipRGCs for whole-cell recording. To minimize photobleaching, the lowest laser power sufficient to reveal somatic GFP labelling was used, and each piece of retina was exposed to this laser for no more than 10 s. Following identification of a GFP-positive soma, the ganglion cell layer was visualized through infrared transillumination, and whole-cell recording was obtained from that soma using a Multiclamp 700B amplifier (Molecular Devices, Sunnyvale, CA, USA). Glass micropipettes with tip resistances 6–8 MΩ were pulled from thick-walled borosilicate tubing on a Narishige PC-10 puller (East Meadow, NY, USA). pCLAMP software (Molecular Devices) was used for data acquisition. Signals were low-pass filtered at 200 Hz and sampled at 1 kHz. Series resistances ranged from ∼15 to ∼30 MΩ and were compensated by 30–40%. Immediately after recording, dye fill of the cell was visualized using epifluorescence and Z-stack images taken at 1 μm steps, and cellular morphology was used to determine cell type as described previously (Hu *et al.* 2013). Briefly, cells with dendrites stratifying exclusively in the 'off' sublamina of the inner plexiform layer were classified as M1. 'On'-stratifying cells with wide dendritic fields and sparse dendrites were categorized as M2. Bistratified cells were M3. Large 'on'-stratifying cells with wide dendritic fields and dense, radially branching dendrites were M4. 'On'-stratifying cells with bushy dendrites and narrow dendritic fields were M5. In order to help distinguish M2 and M4 cells further, Sholl's analysis was used to quantify dendritic density.

In the 'epifluorescence' experiment shown in Fig. 1, ipRGCs were identified through fluorescein isothiocyanate (FITC) epifluorescence imaging of their GFP labelling. The epifluorescence excitation light had emission between ∼450 and ∼490 nm and an intensity of ∼17 log quanta cm^{-2} s^{-1} at the retina, and was presented for ∼10 s onto each piece of retina. Whole-cell recording began 10–15 min after GFP visualization. Postrecording imaging of dye fill was used to determine cell type as explained in the preceding paragraph, and only M4 cells were used in this figure.

In the 'no exposure' experiment shown in Fig. 1 and in the experiment described in Fig. 4*C*, we identified M4 cells under infrared transillumination without GFP imaging,

by targeting the largest somas in the ganglion cell layer for whole-cell recording (Estevez *et al.* 2012). In response to 10 s light steps, some of these cells depolarized transiently or hyperpolarized; they were discarded, because ipRGCs should depolarize in a sustained manner at all stimulus intensities (Fig. 4*A*; Wong *et al.* 2007; Wong, 2012). At the completion of the experiment, the cell was confirmed to be an ipRGC based on its ability to generate depolarizing intrinsic photoresponses in the presence of 50 μM L-AP4, 40 μM DNQX and 25 μM D-AP5. Finally, the dye fill of the cell was imaged to verify its M4-like morphology.

Light stimulation. For the experiment shown in Fig. 8*B*, rightmost column, the stimulus was the above-mentioned FITC epifluorescence light. For all the other experiments, the light source was a miniature OLED monitor (SVGA Rev. 2; eMagin, Bellevue, WA, USA), which had three channels with emission peaks at 439, 515 and 582 nm. This monitor was attached to a filter holder mounted on the camera port of the microscope. The light intensity was adjusted by neutral density filters inserted into the holder. All stimuli were white light generated by activating all three colour channels. To calibrate the intensity of this white light, we first calibrated the intensity of the 515 nm light using a radiometer (Gamma Scientific, San Diego, CA, USA) and then compared the responses of six ipRGCs to an intensity series of the white light *vs.* an intensity series of the 515 nm light. The unattenuated 515 nm light was measured to be 13.1 log quanta cm^{-2} s^{-1}, and the six cells were ~0.4 log units more sensitive to the white light than to the 515 nm light; thus, the unattenuated white light was equivalent to 13.5 log quanta cm^{-2} s^{-1} of 515 nm light. All photon fluxes in the text are expressed as equivalent 515 nm light. Stimuli were programmed in Matlab using the Psychophysics Toolbox (Brainard, 1997) and delivered to the retina through the objective lens.

In the receptive field-mapping experiment (Fig. 6), the stimuli were light spots centred over each cell's receptive field. To locate the receptive field centre, a light spot of 200 ms duration and 200 μm diameter was presented at different positions, and the position inducing the largest response was determined. Spatial mapping of the receptive field was conducted as follows: for each cell, 200–400-ms-duration spots with seven or eight different diameters were presented in a random order at 5 s intervals, and the first diameter was presented again at the end of the experiment to confirm recording stability. In the experiment testing responses to moving light bars (Fig. 7), all light bars were 100 μm thick and 4 mm long, and each stimulus traversed the entire piece of retina. In the direction selectivity experiment (Fig. 7*A*), the light bars moved at 18 deg s^{-1}. In all the other experiments, the stimuli were full-field light.

Data analysis. To measure resting membrane potentials, recordings made in darkness were low-pass filtered offline at 20 Hz to filter out all the spikes. To measure photoresponse amplitudes, the recordings were also low-pass filtered offline at 20 Hz, and amplitudes were then measured relative to the prestimulus baseline. In the experiment described in Fig. 7*A*, the direction selectivity index (DSI) for each cell was calculated as follows. First, the DSI for each of the four axes of motion was calculated using the expression $(x-y)/(x+y)$, where x and y represent the amplitudes of the larger and smaller responses, respectively. Then, the largest of the four DSI values was selected as the DSI for the cell. Statistical analyses of two data groups were performed using Student's t test (unpaired for the comparisons shown in Figs. 1 and 6*C*; paired for those shown in Fig. 7*B*), whereas comparisons of more than two groups were made using one-way ANOVA followed by Tukey's *post hoc* tests. For all statistical comparisons, the significance level was set at a P value of 0.05. All error bars represent SEM.

Difference-of-Gaussians fitting. The sizes of the centre and surround components of the bipolar- and amacrine-input receptive fields were estimated by fitting the amplitude *vs.* spot diameter plots (Fig. 6*B*) with a difference-of-Gaussians centre–surround model, as follows (Rodieck, 1965; Einevoll & Plesser, 2005):

$$R_{\text{spot}}(r) = k_c[1 - \exp(-r^2/4\sigma_c^2)] - k_s[1 - \exp(-r^2/4\sigma_s^2)]$$

where k_c and k_s are the peak amplitudes of the centre and surround components, σ_c and σ_s are the space constants of the centre and surround, and r is the spot radius. The response of each cell was fitted independently, and mean values of k_c, k_s, σ_c and σ_s were used to generate the centre and surround Gaussians shown in Fig. 6*C*.

Retrograde labelling from the superior colliculus

The *Opn4*$^{Cre/+}$*;GFP* mice were anaesthetized with isoflurane (3% in oxygen), placed in a stereotaxic apparatus, and body temperature was maintained using a heating pad. An incision was made in the scalp to expose the skull over the lambdoid suture, and two holes were manually drilled in the skull using a 21 gauge needle immediately anterior to the suture, each about 0.5 mm lateral to the mid-line. Cholera toxin β-subunit conjugated to Alexa Fluor594 (~1 μl of a 5 μg ml^{-1} PBS solution; Life Technologies) was injected by hand through each hole using a micropipette coupled to a manual pressure source. Three to five days after injection, mice were killed by CO_2 inhalation and pneumothorax. Both retinas were isolated, and whole-cell recordings were made from Alexa594-stained, GFP-positive ganglion cells to fill these cells with Lucifer Yellow for morphological analysis. To confirm accuracy of the injection, the brain was removed, submerged

in 4% paraformaldehyde overnight, rinsed with PBS, cryoprotected in 30% sucrose, frozen in OCT (optimal cutting temperature) medium, and sectioned at 100 μm on a freezing microtome in the sagittal plane. Injection sites were assessed by epifluorescence microscopy.

Results

Multiphoton imaging of GFP labelling minimizes photobleaching

This study employed *opn4*$^{Cre/+}$*;GFP* mice, in which ipRGCs are selectively labelled with GFP (Ecker *et al.* 2010), and we used a 915 nm multiphoton laser to image GFP labelling. This laser was delivered at the lowest power sufficient to reveal GFP signals on the computer monitor, and was presented to each piece of retina for no more than 10 s. To assess the effectiveness of this imaging method in preserving the dark-adapted state of ipRGCs, we compared the behaviours of cells identified using this multiphoton laser *vs.* those identified without any laser. We focused this analysis on M4-type ipRGCs because their large somas enable them to be targeted easily without GFP visualization (see Methods). In darkness, the two cell groups had virtually identical resting membrane potentials (Fig. 1*A*; $P = 0.996$) and spontaneous firing frequencies (Fig. 1*B*; $P = 0.980$). Furthermore, their responses to an intensity series of 10 s full-field light had impressively similar waveforms (Fig. 1*C*), peak amplitudes at light onset (Fig. 1*D*; $P > 0.05$ for 7.5–11.5 log quanta cm^{-2} s^{-1}) and trough amplitudes at light offset (Fig. 1*E*; $P > 0.05$ for 7.5–11.5 log quanta cm^{-2} s^{-1}). These observations demonstrated that ipRGCs remain well dark adapted following our low-intensity and short-duration multiphoton imaging of GFP labelling.

In contrast, epifluorescence imaging of GFP labelling substantially altered the behaviours of M4 cells. While their resting potentials were not significantly different from those of the 'no exposure' cells (Fig. 1*A*; $P = 0.40$),

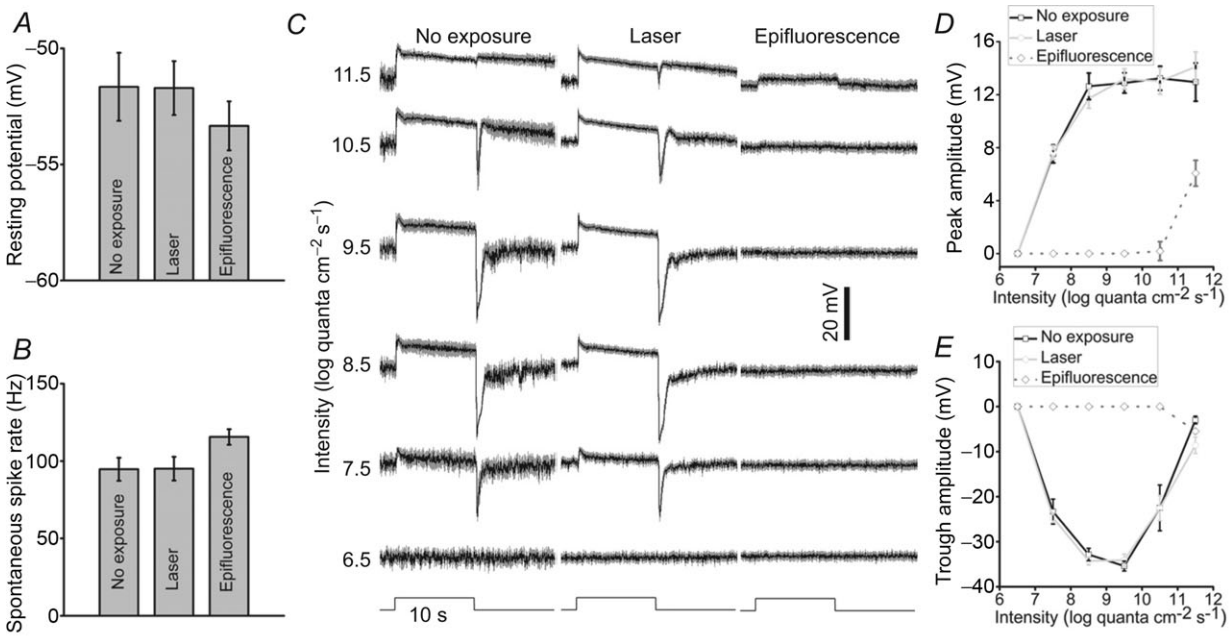

Figure 1. Multiphoton-targeted intrinsically photosensitive retinal ganglion cells (ipRGCs) are physiologically indistinguishable from dark-adapted ipRGCs
These experiments compared the resting membrane potentials, spontaneous spike rates and light responses of M4-type ipRGCs identified using the following three different methods: without exposure to any laser or epifluorescence ('no exposure'); 915 nm multiphoton laser ('laser'); and fluorescein isothiocyanate (FITC) epifluorescence ('epifluorescence'). *A*, in darkness, the 'no exposure' and 'laser' cell groups had virtually identical resting potentials. Although the epifluorescence-targeted cells were somewhat more negative than the 'no exposure' cells, the difference was insignificant ($P > 0.05$). Error bars represent SEM. *B*, in darkness, the first two groups spiked spontaneously at similar rates, whereas the epifluorescence-targeted group spiked at a significantly higher rate ($P < 0.05$ *vs.* 'no exposure'). *C*, averaged responses (black traces) of the three cell groups to an intensity series of full-field, 10-s-duration light steps, with all spikes filtered out. The grey regions around the black traces represent SEM. Notice the striking similarity of the waveforms of the first two cell groups. *D*, averaged peak amplitudes of the light-on responses. *E*, averaged trough amplitudes of the light-off responses. In all panels, $n = 5$ for the 'no exposure' cells, $n = 17$ for the 'laser' cells and $n = 13$ for the 'epifluorescence' cells.

spontaneous spike rates were elevated (Fig. 1*B*; $P < 0.05$) and photoresponses dramatically attenuated (Fig. 1*C*), in terms of both their peak amplitudes (Fig. 1*D*; $P < 0.05$ for 7.5–11.5 log quanta cm^{-2} s^{-1}) and trough amplitudes (Fig. 1*E*; $P < 0.05$ for 7.5–10.5 log quanta cm^{-2} s^{-1}).

Resting properties

In all the electrophysiological experiments presented in this paper, the retinas were kept in constant darkness except during stimulus presentation, and we noticed that in the absence of light, different ipRGC types had varied resting membrane potentials and spontaneous spike rates. Thus, we first examined these resting properties in some detail. Schmidt & Kofuji (2010) had previously reported the resting potentials of M1 and M2 cells; however, those cells were partly light adapted, and M3–M5 cells were not investigated. In the dark, the resting potentials of multiphoton-targeted ipRGCs ranged from -61.5 ± 1.5 mV for M3 cells to -51.7 ± 1.2 mV for M4 cells (Fig. 2*A* and *B*), and the differences between the following cell types were statistically significant: M1 *vs.* M2 ($P = 0.025$); M1 *vs.* M4 ($P < 0.001$); M2 *vs.* M3 ($P = 0.002$); and M3 *vs.* M4 ($P < 0.001$). All cells spiked spontaneously in darkness, with firing rates ranging from 8.4 ± 2.6 Hz for M1 to 95.1 ± 7.7 Hz for M4 (Fig. 2*A* and C), and these ipRGC pairs were significantly different, as follows: M1 *vs.* M2 ($P = 0.001$); M1 *vs.* M4 ($P < 0.001$); M1 *vs.* M5 ($P < 0.001$); M2 *vs.* M4 ($P < 0.001$); M2 *vs.* M5 ($P = 0.03$); M3 *vs.* M4 ($P < 0.001$); and M3 *vs.* M5 ($P = 0.007$).

Intrinsic light responses

Given that our multiphoton-targeted ipRGCs are significantly more dark adapted than those in most previous studies and that the intrinsic light responses of M5 cells had not been described in detail (Ecker *et al.* 2010), we sought to re-examine the intrinsic photoresponses of all five ipRGC types in dark-adapted conditions. To record the intrinsic light response in isolation, we blocked rod/cone signalling using 50 μM L-AP4 (mGluR6 agonist), 40 μM DNQX (AMPA/kainate receptor antagonist) and 25 μM D-AP5 (NMDA receptor antagonist; Fig. 3*A*). We confirmed that in the presence of these drugs, the responses of M1 cells to full-field light were depolarizing at all intensities (Berson *et al.* 2002; Wong *et al.* 2005; Fig. 3*B*, column 1). For M2–M5 cells, however, response polarity depended on stimulus intensity: they were depolarizing for intensities exceeding ~12 log quanta cm^{-2} s^{-1}, but slightly

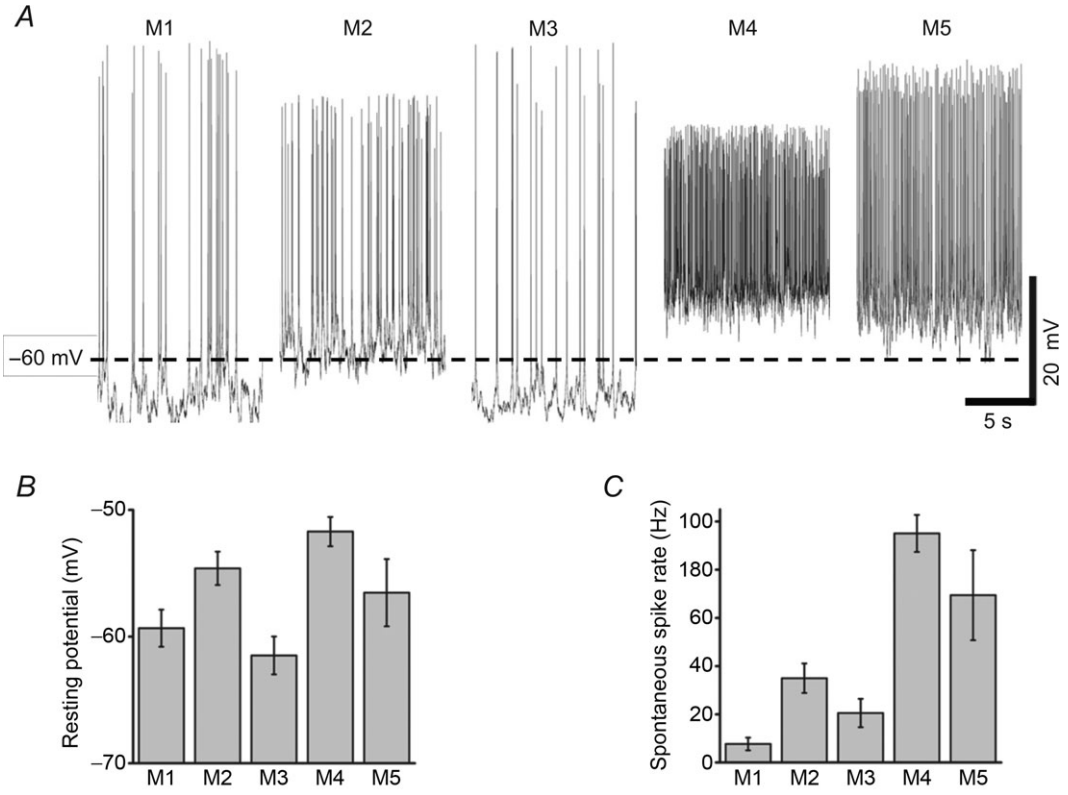

Figure 2. Resting potentials and spontaneous spike rates
A, representative examples of current-clamp recordings made from the five types of ipRGCs in darkness. *B*, averaged resting membrane potentials. *C*, averaged spontaneous spike rates. For *B* and *C*, M1 cells, $n = 12$; M2, $n = 17$; M3, $n = 12$; M4, $n = 17$; and M5, $n = 7$.

hyperpolarizing for lower intensities (Fig. 3*B*, columns 2–5). These low-amplitude hyperpolarizing photoresponses persisted in melanopsin-knockout ipRGCs and could also be observed in conventional ganglion cells during rod/cone signalling blockade (Supporting information Fig. S1); thus, they were probably field potentials derived from rod/cone photoreceptors and will not be discussed further.

By studying M1–M4 cells, previous researchers reported that the thresholds, amplitudes and kinetics of intrinsic ipRGC photoresponses were cell type dependent (Schmidt & Kofuji, 2009, 2011; Ecker *et al.* 2010; Estevez *et al.* 2012).

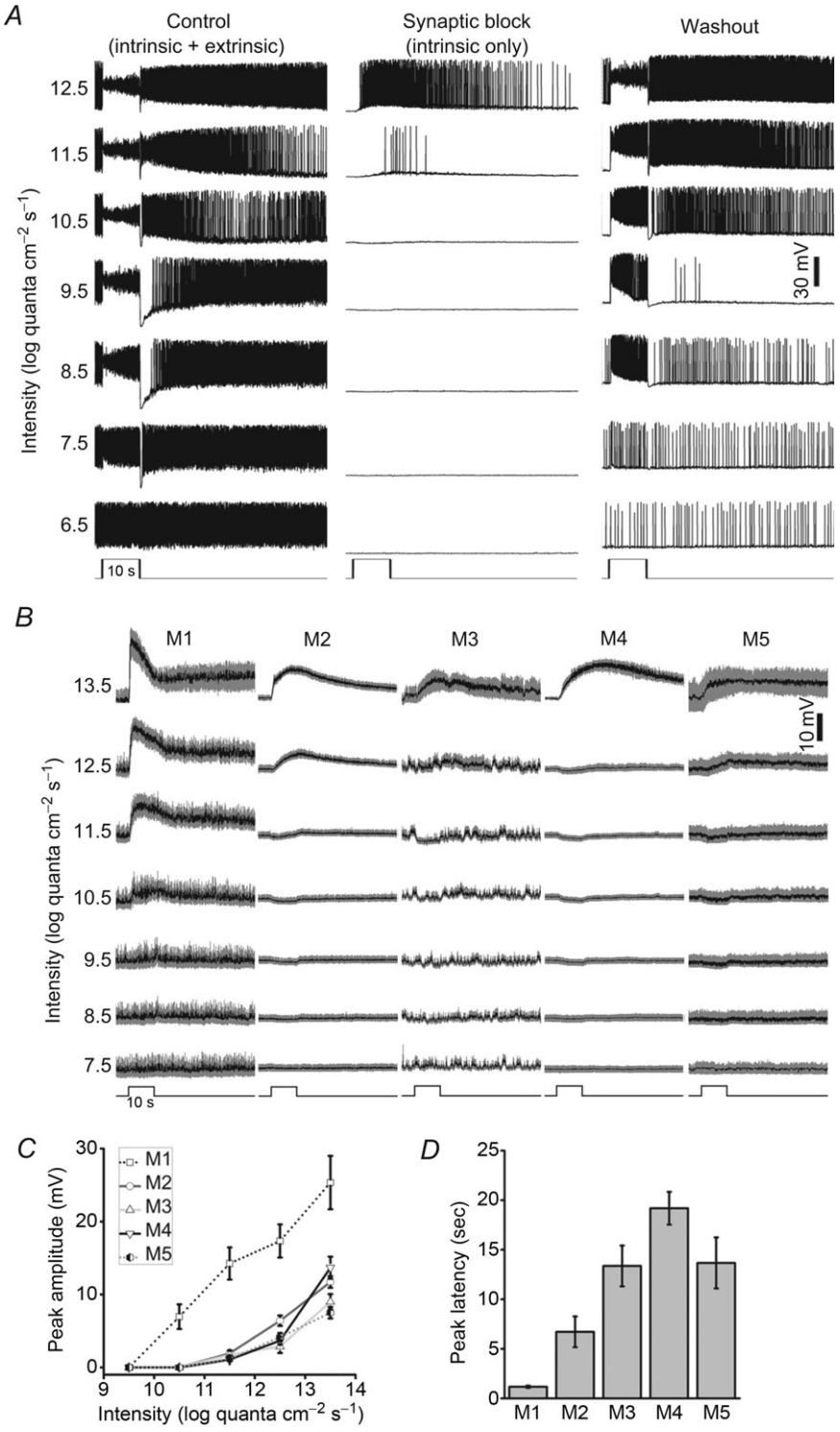

Figure 3. Intrinsic, melanopsin-mediated light responses
A, example current-clamp recordings from an M2 cell. In the left traces, when superfused with normal Ames' medium, both intrinsic (melanopsin-based) and extrinsic (synaptically mediated) light responses were permitted. In the middle traces, in the presence of 50 μM L-(+)-2-amino-4-phosphonobutyric acid (L-AP4), 40 μM 6,7-dinitroquinoxaline-2,3-dione (DNQX) and 25 μM D-(−)-2-amino-5-phosphonopentanoic acid (D-AP5), only the intrinsic photoresponses remained, which were several log units less sensitive than the extrinsic light responses. The right traces show that extrinsic light responses returned after washout of the drugs. *B*, averaged intrinsic light responses of the five types of ipRGCs recorded under current clamp in the presence of L-AP4, DNQX and D-AP5, with all spikes filtered out. Note that for M2–M5 cells, light intensities between 8.5 and 11.5 log quanta cm^{-2} s^{-1} evoked small hyperpolarizing responses (see Supporting information for further information). *C*, averaged peak amplitudes, measured from the prestimulus baseline to the most depolarized point in the light response. *D*, averaged peak latencies of the intrinsic responses to the 13.5 log quanta cm^{-2} s^{-1} light step. In *B–D*, for M1, $n = 4$–10; M2, $n = 10$–14; M3, $n = 5$–7; M4, $n = 4$–9; and M5, $n = 2$–4.

We examined all five morphological types and confirmed that the intrinsic light responses of M1 cells had the lowest thresholds and the highest peak amplitudes. We further found M2–M5 cells to have fairly similar peak amplitude *vs.* intensity relationships (Fig. 3*C*), with insignificant across-type differences at 11.5 (ANOVA $P = 0.355$) or 13.5 log quanta cm^{-2} s^{-1} (ANOVA $P = 0.073$), although the responses to 12.5 log quanta cm^{-2} s^{-1} were significantly different between M2 and M3 ($P = 0.020$) and between M2 and M4 ($P = 0.040$). In terms of response kinetics, a wide range of peak latencies was observed (ANOVA $P < 0.001$), with the shortest latency for M1 cells and the longest for M4 cells (Fig. 3*D*), in agreement with a previous study (Ecker *et al.* 2010). Significant differences were observed between the latencies of M1 *vs.* M2 ($P = 0.001$), M1 *vs.* M4 ($P < 0.001$), M1 *vs.* M5 ($P < 0.001$), M2 *vs.* M4 ($P < 0.001$), M2 *vs.* M5 ($P = 0.03$), M3 *vs.* M4 ($P < 0.001$) and M3 *vs.* M5 ($P = 0.007$).

Extrinsic light responses

To analyse extrinsic photoresponses, we recorded from ipRGCs in normal Ames' medium to preserve rod/cone signalling and presented full-field light steps with intensities ranging from 6.5 to 9.5 log quanta cm^{-2} s^{-1}, which were below the threshold for inducing melanopsin responses (Fig. 3*B*). Earlier studies had found the extrinsic photoresponses of epifluorescence-targeted and hence partly light-adapted M1 cells to be significantly more transient and smaller than those of M2 and M4 cells (Wong *et al.* 2007; Schmidt & Kofuji, 2010; Estevez *et al.* 2012). In contrast, our recordings of dark-adapted ipRGCs showed that the five cell types generated remarkably similar responses to full-field light steps (Fig. 4*A*). Specifically, for all five types, the threshold intensity was between 6.5 and 7.5 log quanta cm^{-2} s^{-1}. The responses of all cells were depolarizing and peaked almost instantaneously at light onset. After peaking, all responses decayed over time, but all cells remained depolarized relative to baseline during the remainder of the light step. At light offset, all cells hyperpolarized transiently before returning gradually to the resting membrane potential. In contrast, the peak amplitudes of these light responses varied among ipRGC types (ANOVA $P < 0.05$ for the 7.5, 8.5 and 9.5 log intensities), with M1 and M3 having the highest amplitudes, M2 having intermediate amplitudes, and M4 and M5 showing the smallest peak responses (Fig. 4*B*, left plot). To quantify the rates at which the five cell types adapt to steady light, we measured the amplitudes of their responses near the end of the light steps (Fig. 4*B*, middle plot) and calculated the ratios of these amplitudes to the peak amplitudes (Fig. 4*B*, left plot), and found the ratios to be statistically indistinguishable for all five cell types (Fig. 4*B*, right plot; ANOVA $P > 0.05$ for all light intensities), suggesting similar time courses of response decay.

The epifluorescence used in previous studies to target ipRGCs severely bleached rhodopsin, precluding an assessment of rod input. In the present investigation, the high sensitivity of extrinsic light responses (Fig. 4*A*) suggested that all ipRGCs might receive input from rods. To test this possibility, we determined the threshold intensities of ipRGCs in *Gnat1*$^{-/-}$ mice, which lack rod function (Calvert *et al.* 2000). As ipRGCs are not labelled in these mice, we recorded only from M4 cells, which could be identified without GFP imaging (see Methods). In *Gnat1*$^{-/-}$ mice, the threshold intensity for M4 cells was between 8.5 and 9.5 log quanta cm^{-2} s^{-1} (Fig. 4*C*, left traces), roughly 2 log units higher than for ipRGCs in *opn4*$^{Cre/+}$*;GFP* mice (Fig. 4*A*), indicating that the responses of the latter cells to the 7.5 and 8.5 log intensities could not be due to cone input. As a confirmation, we also recorded from M4 cells in *Gnat2*^{cpfl3} mice, which lack cone function (Chang *et al.* 2006), and determined their threshold intensity to be between 6.5 and 7.5 log quanta cm^{-2} s^{-1} (Fig. 4*C*, right traces), matching that for ipRGCs in *opn4*$^{Cre/+}$*;GFP* mice. In conclusion, all types of ipRGCs generate rod-driven light responses.

A previous study of epifluorescence-targeted rat M1 cells showed that their extrinsic photoresponses were dominated by inhibitory GABAergic/glycinergic input from 'on' amacrine cells, with excitatory glutamatergic input from 'on' bipolar cells triggering much weaker light responses (Wong *et al.* 2007). In the next experiment, we re-examined these two inputs for all five types of mouse ipRGCs, using dark-adapted cells. To record inhibitory light responses in isolation, ipRGCs were voltage clamped at +3 mV, the reversal potential for cationic input (E_{cations}) to these ganglion cells (Hu *et al.* 2013), whereas to record excitatory light responses, cells were voltage clamped at −70 mV, near the reversal potential for Cl^- (E_{Cl}). We found that bipolar and amacrine inputs evoked light responses of comparable peak amplitudes and that the bipolar-driven responses tended to be more sustained than the amacrine-driven ones (Fig. 5). Although both inputs evoked conductance increases during the light step for all cell types, the amacrine-driven responses of M1 and M3 cells (but not the other ipRGCs) also included a conductance increase at light offset (Fig. 5, arrows), which had not been detected for light-adapted rat M1 cells (Wong *et al.* 2007).

Receptive field organization

All the experiments discussed so far tested full-field lights. Given that there is emerging evidence suggesting a role for ipRGCs in image-forming vision (Brown *et al.* 2010; Ecker *et al.* 2010), the next experiments tested more complex stimuli to investigate the sensitivity of these neurons to

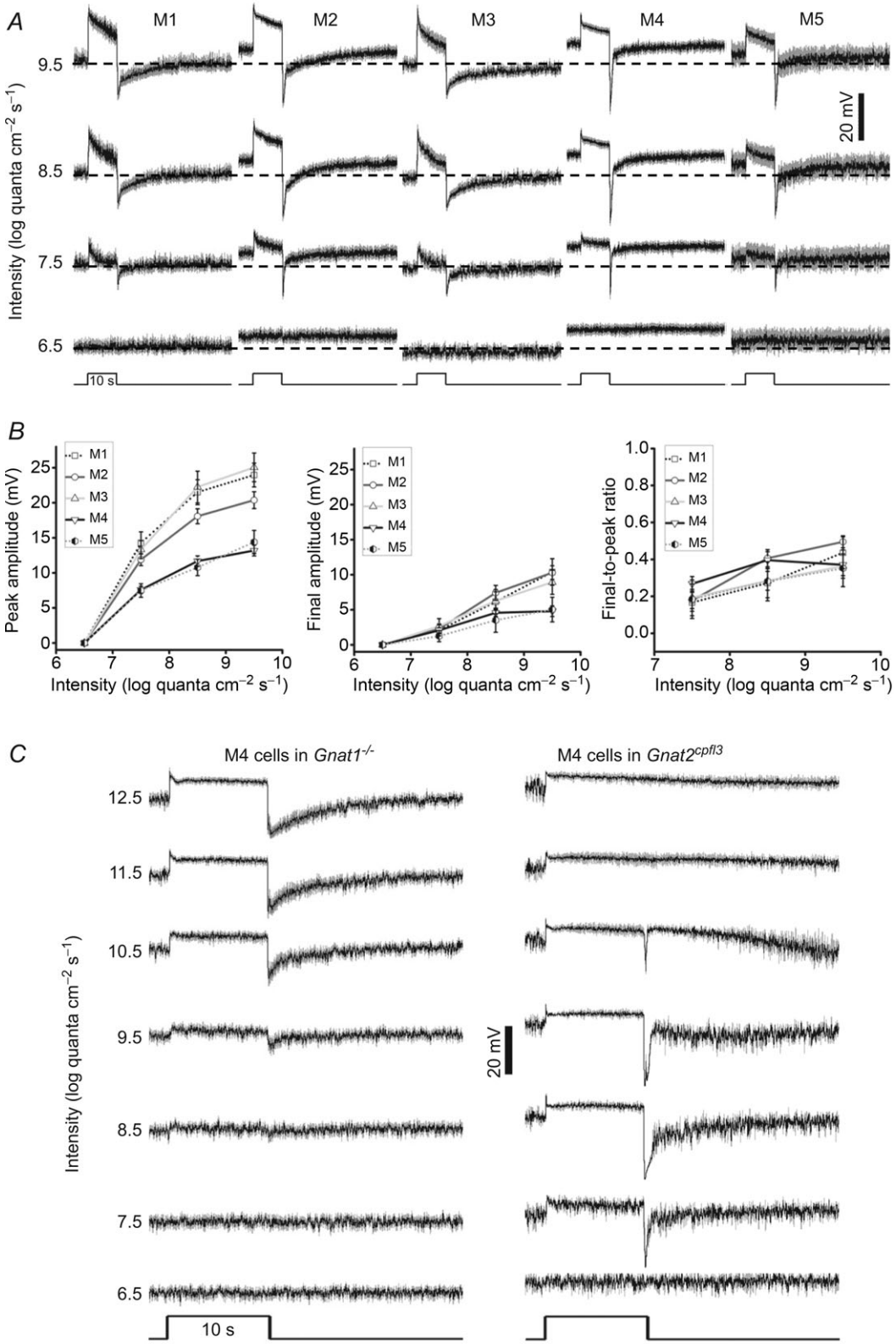

spatial contrast and motion. To examine spatial contrast sensitivity, we studied the voltage responses of ipRGCs to different sizes of light spots centred within each cell's receptive field to probe for centre–surround antagonism. For M1 cells, response amplitude increased as the spot diameter increased from 100 to 500 μm but remained unchanged as the diameter exceeded 500 μm, indicating the absence of an antagonistic surround region (Fig. 6*A*, top plot). In contrast, the responses of all other ipRGCs peaked when the spot diameter reached between 200 and 500 μm and became progressively smaller for larger spots, indicating that the receptive fields of M2–M5 cells have antagonistic surrounds (Fig. 6*A*, second to fifth plots).

Given that M1 cells showed no obvious surround interaction in the above experiment, we then mapped the bipolar and amacrine inputs separately using voltage-clamp recordings to assess whether these inputs also lacked surround inhibition. Although amacrine-driven responses of M1 cells to prolonged light steps exhibited conductance increases at light offset as well as onset (Fig. 5), for the brief stimuli (200–400 ms in duration) used in this mapping experiment, the light-off responses were too small to be measured reliably and so we analysed only the light-on responses. To our surprise, we found that the receptive fields for both the 'on' bipolar and the 'on' amacrine inputs exhibited pronounced centre–surround antagonism (Fig. 6*B*). Thus, the lack of an obvious surround in the current-clamp recordings of M1 cells (Fig. 6*A*, top plot) is probably due to the surround inhibition of the amacrine input masking the surround inhibition of the bipolar input. In other words, as a larger area of the surround region becomes illuminated by a larger spot, the influences of the excitatory and inhibitory inputs decrease more or less concurrently, thereby obscuring the presence of an antagonistic surround.

Notice that in Fig. 6*B*, the averaged 'on' amacrine-driven response peaked at the 50 μm spot diameter, whereas the 'on' bipolar-driven response peaked at 200 μm, suggesting that the two inputs may have different spatial profiles. To estimate the spatial extents of the centre and surround regions of each input, the difference-of-Gaussians model (Rodieck, 1965; Einevoll & Plesser, 2005) was used to fit these responses (dotted curves in Fig. 6*B*), to generate one Gaussian function describing the centre response and another that describes the surround response (Fig. 6*C*). The averaged space constant of the 'on' amacrine input's 'centre' Gaussian function was 14 ± 3.6 μm, which was significantly smaller than that for the ON bipolar input, 34 ± 3 μm ($P = 0.001$). Likewise, the 'on' amacrine input's 'surround' space constant of 63 ± 14 μm was significantly smaller than that of the 'on' bipolar input, 218 ± 46 μm ($P = 0.006$).

Responses to moving stimuli

We next investigated the motion sensitivity of ipRGCs by examining their voltage responses to moving light bars. It was previously reported that SCN-projecting ganglion cells in cats responded strongly to non-moving or extremely slow-moving stimuli ($\sim$3 deg s^{-1}) but poorly to higher speeds (Pu, 2000) and that the responses of mouse M4 cells to moving lights were not directionally selective (Estevez *et al.* 2012). By presenting light bars moving in eight different directions, we found that all multiphoton-targeted ipRGCs had direction selectivity indices below 0.1 (Fig. 7*A*), indicating that none of them was directionally selective. However, because some non-directionally selective ganglion cells could still analyse the speed of motion (Barlow *et al.* 1964; Lee & Willshaw, 1978; Cohen *et al.* 1980; Frechette *et al.* 2005), we next examined whether ipRGCs might have this ability by testing light bars moving at six different speeds, i.e. 0.72, 1.8, 7.2, 18, 72 and 180 deg s^{-1}. All ipRGCs responded robustly to each speed. For M1–M4, responses to some of the intermediate speeds were significantly larger than those to the lowest speed ($P < 0.05$), and different cell types had different speed preferences, with M1 and M3 responding most strongly to the 7.2 deg s^{-1} light bar, M2 to the 18 deg s^{-1} light and M4 cells to the 72 deg s^{-1} light (Fig. 7*B*).

Projection to the superior colliculus

The centre–surround receptive fields of M2–M5 cells and the different speed tuning properties of the various morphological types suggested the possibility that these cells contribute to spatial and motion analyses. Consistent with this notion, many non-M1-type ipRGCs, including

Figure 4. Extrinsic, synaptically driven light responses
A, averaged responses of the five ipRGC types to light steps too dim to induce depolarizing intrinsic photoresponses. The horizontal dashed lines indicate a membrane potential of −60 mV. All spikes have been filtered out. For M1, $n = 12$; M2, $n = 17$; M3, $n = 12$; M4, $n = 17$; and M5, $n = 7$. *B*, analysis of the data shown in *A*. Left panel shows peak response amplitudes at light onset. Middle panel shows final photoresponse amplitudes, measured 0.1 s before the end of the 10 s light step. Right panel shows ratios of the final amplitudes to the peak amplitudes. *C*, to determine whether ipRGCs generate rod-driven light responses, we compared the light responses of M4 cells in *Gnat1*$^{-/-}$ mice (left traces; $n = 9$) *vs.* those of M4 cells in *Gnat2*^{cpfl3} mice (right traces; $n = 2$). With rod function abolished in the *Gnat1*$^{-/-}$ mice, the threshold intensity was elevated from 7.5 to 9.5 log quanta cm^{-2} s^{-1}, whereas the threshold remained at 7.5 log quanta cm^{-2} s^{-1} when cones were silenced in the *Gnat2*^{cpfl3} mice, indicating that ipRGCs can generate rod-mediated light responses.

M4 cells, project to the dorsal lateral geniculate nucleus (dLGN) of the primary image-forming visual pathway (Ecker *et al.* 2010; Estevez *et al.* 2012). Furthermore, ipRGCs prominently innervate the SC (Hattar *et al.* 2006; Ecker *et al.* 2010; Galindo-Romero *et al.* 2013), a sensorimotor area that orients the gaze towards novel stimuli and that provides a secondary route for visual information to reach the cortex. In the next experiment, we sought to determine which types of ipRGCs project to the SC. We injected Alexa594-conjugated cholera toxin β-subunit into the SC of 11 *opn4*$^{Cre/+}$*;GFP* mice (Fig. 8*A*) and filled retrolabelled GFP-positive cells with Lucifer Yellow to analyse their morphologies and determine their cell types. A total of 20 such cells were found and successfully filled, of which 10 were M1, six M2, two M3 and two M4 (Fig. 8*B*, first four columns). All cells generated intrinsic light responses in the presence of 50 μM L-AP4, 40 μM DNQX and 25 μM D-AP5 (Fig. 8*B*, rightmost column), confirming that they were ipRGCs.

Discussion

Using multiphoton microscopy to image GFP preserves the dark-adapted state of retinal neurons

The use of genetically encoded fluorescent proteins has greatly facilitated the studies of numerous biological processes, including electrophysiological analyses of various neuronal cell types. Several laboratories have created mouse lines in which ipRGCs are selectively labelled with fluorescent proteins to enable targeted single-cell recording. In nearly all studies of ipRGCs published to date, epifluorescence was used to image labelled cells, thus light adapting them and preventing an assessment of their dark-adapted behaviour. Here, we have overcome this limitation by using a multiphoton laser to identify GFP-labelled ipRGCs. The ability of multiphoton imaging to minimize photobleaching has been widely assumed, but the result shown in Fig. 1 is the first definitive demonstration that the dark-adapted state of retinal cells can be preserved reasonably well if GFP is imaged in this way. All the multiphoton-targeted cells used in this study were exposed to the laser for no more than 10 s, and the lowest intensity that revealed GFP signals was used. We have noticed that longer exposure durations or higher laser intensities tend to elevate the thresholds of ipRGC photoresponses significantly, suggesting that excessive multiphoton exposures can cause substantial bleaching of photopigments (Euler *et al.* 2009).

Resting properties

We have made the first measurements of the resting membrane potentials of M3–M5 cells in normal Ames' medium with synaptic input intact. The resting potentials of epifluorescence-targeted M1 and M2 cells had been

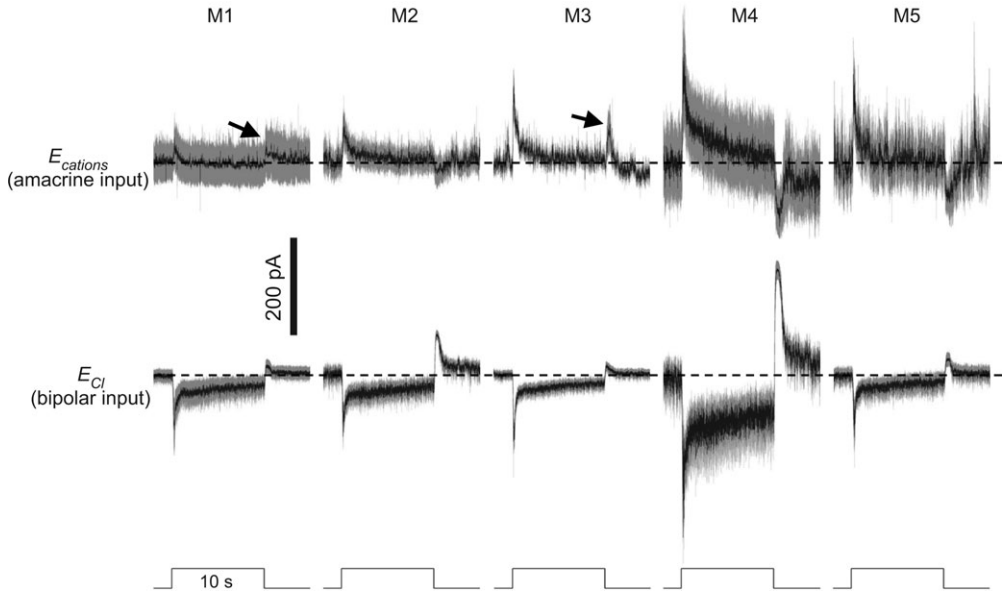

Figure 5. Bipolar cell-driven *vs.* amacrine cell-driven light response
All light stimuli were 8.5 log quanta cm^{-2} s^{-1}, below the threshold intensity for inducing melanopsin responses. In the top traces, to analyse amacrine-driven light responses in isolation, ipRGCs were voltage clamped at the reversal potential for cationic input ($E_{cations}$). The arrows highlight light-off conductance increases detected in M1 and M3 cells, the only ipRGC types that possess dendrites in the 'off' sublamina of the inner plexiform layer. For M1, $n = 5$; M2, $n = 12$; M3, $n = 9$; M4, $n = 9$; and M5, $n = 4$. In the bottom traces, to record bipolar-driven light responses, ipRGCs were voltage clamped at the reversal potential for chloride (E_{Cl}). For M1, $n = 10$; M2, $n = 10$; M3, $n = 13$; M4, $n = 8$; and M5, $n = 4$. The horizontal dashed lines indicate prestimulus baselines.

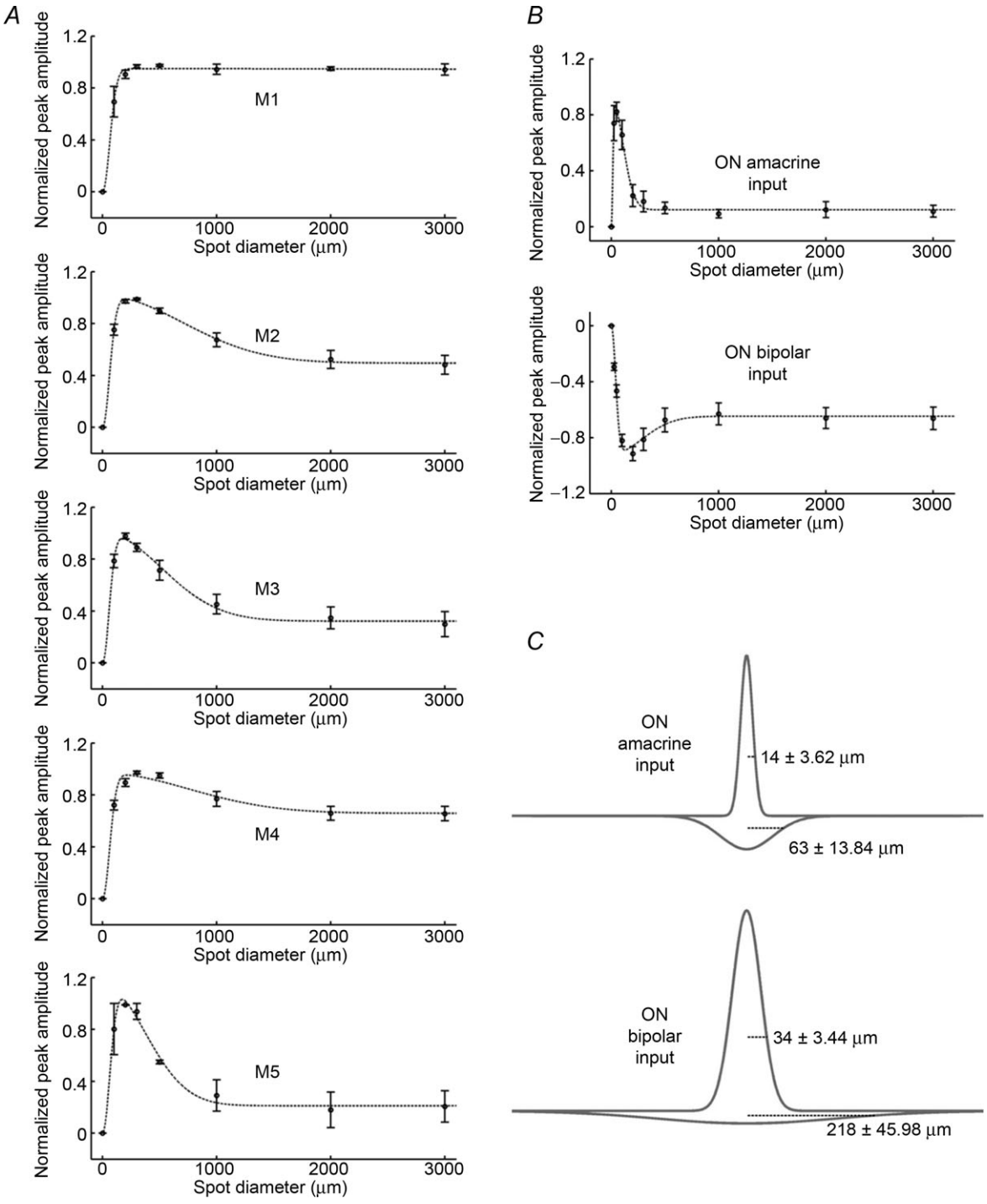

Figure 6. Receptive field organization
A, the current-clamp responses of different ipRGC types to light spots of various diameters, with the largest response of each cell normalized to 1. The dotted lines are difference-of-Gaussians fits of the data. Light intensity was 9.8 log quanta cm^{-2} s^{-1}. For M1, $n = 4$; M2, $n = 10$; M3, $n = 7$; M4, $n = 10$; and M5, $n = 2$. *B* shows, for M1 cells, the normalized 'on' amacrine-driven (top plot) and 'on' bipolar-driven responses (bottom plot) to light spots of various diameters, recorded by voltage clamping at $E_{cations}$ and E_{Cl}, respectively. The dotted lines are difference-of-Gaussians fits of the data. Light intensity was 9.8 log quanta cm^{-2} s^{-1}. For both inputs, $n = 8$. *C* shows, for M1 cells, the Gaussian functions describing the centre (upward curves) and surround regions (downward curves) of 'on' amacrine-driven (top plot) and 'on' bipolar-driven receptive fields (bottom plot). The distance values indicate the space constants of the Gaussian fits.

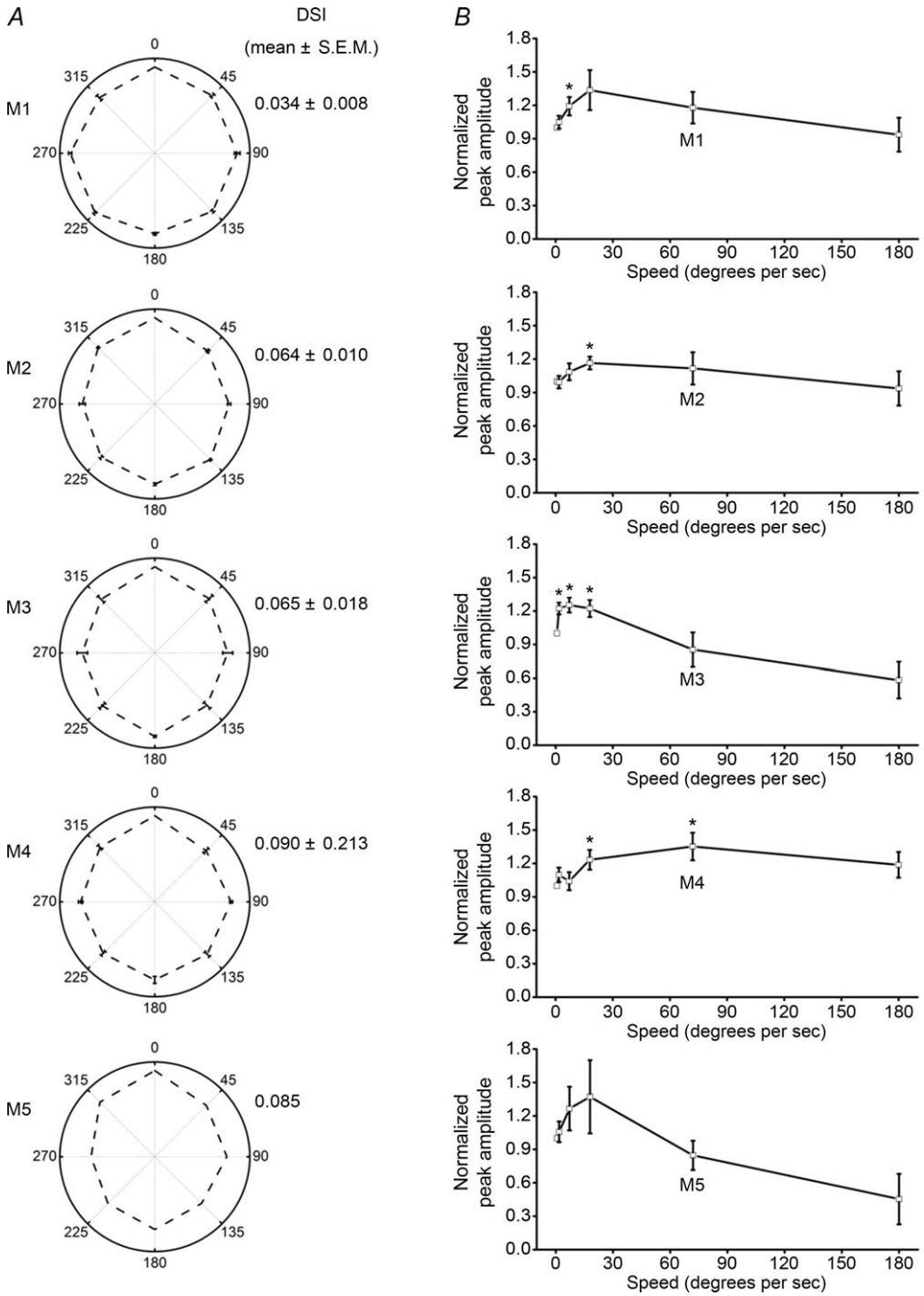

Figure 7. Responses to moving lights
All ipRGCs responded robustly to moving stimuli, with M1–M4 exhibiting speed tuning, although none of them was directionally selective. *A*, averaged responses of ipRGCs to light bars drifting in eight different directions. For each cell tested, the motion direction causing the largest response was set at 0 deg in these plots, and the response amplitudes for the other directions were normalized to this response. The direction selectivity indices (DSI) are shown to the right of the plots. For M1, $n = 2$; M2, $n = 10$; M3, $n = 6$; M4, $n = 7$; and M5, $n = 1$. *B*, the responses of ipRGCs to light bars moving at different speeds. The response amplitudes for each cell were normalized to its response to the lowest speed (0.72 deg s^{-1}). Asterisks indicate response amplitudes that were significantly different from the 0.72 deg s^{-1} responses (*P* values were between 0.014 and 0.046). For M1, $n = 9$; M2, $n = 7$; M3, $n = 5$; M4, $n = 8$; and M5, $n = 3$. For both *A* and *B*, all recordings were made under current clamp, and the intensity of all light bars was 9.8 log quanta cm^{-2} s^{-1}.

measured by Schmidt & Kofuji (2010), who found the former to be about 5 mV more depolarized than the latter. In contrast, our dark-adapted M1 cells are significantly more hyperpolarized than M2 cells, by about 5 mV (Fig. 2*B*), suggesting that the resting potentials of ipRGCs may depend on their adaptational state. In addition, we have made the first measurements of the spontaneous spike rates of all five cell types in normal Ames' medium and have shown that this property may also be affected by an ipRGC's adaptational state (Fig. 1*B*). In

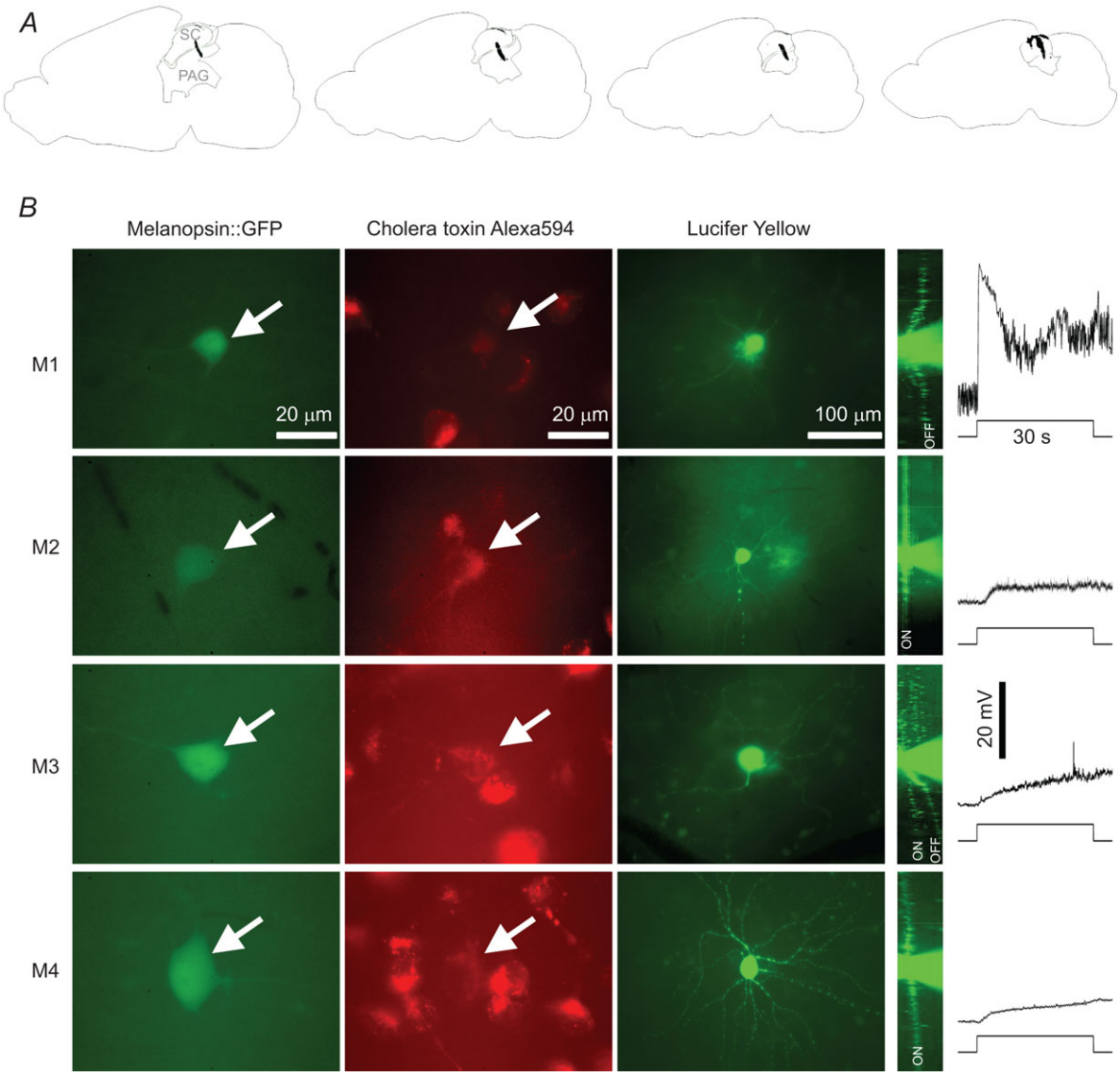

Figure 8. The M1–M4 cells project to the superior colliculus
To determine which ipRGC types project to the superior colliculus (SC), Alexa594-conjugated cholera toxin β-subunit was injected bilaterally into the SC of *opn4*$^{Cre/+}$*;GFP* mice, and the morphologies of retrolabelled green fluorescent protein (GFP)-positive retinal ganglion cells were examined. *A*, fluorescence images of an animal's injection site were superimposed on anatomical drawings adapted from the Allen mouse brain atlas (http://mouse.brain-map.org/). Sections are mid-line to lateral from left to right and separated by 100 μm. For all injected animals, some of the tracer dye was deposited into the periaqueductal grey (PAG), which does not receive direct retinal input. *B*, M1–M4 cells could be retrolabelled from the SC. These are examples of retrolabelled cells from four different pieces of retina. Column 1, GFP fluorescence indicating ipRGC somas. Column 2, Alexa594 staining of the retrogradely transported cholera toxin β-subunit. The arrows highlight the GFP-labelled somas shown in column 1. Column 3, Z-stack projections of the Lucifer Yellow fills of these cells. Column 4, the Z-stacked images of the Lucifer Yellow fills were rotated 90 deg to show the cells' dendritic stratification patterns. 'ON' and 'OFF' indicate the 'on' and 'off' sublaminas of the inner plexiform layer, respectively. Column 5, the intrinsic light responses of these cells recorded in the presence of L-AP4, DNQX and D-AP5, with all spikes filtered out. The stimulus was a FITC epifluorescence light source and had an intensity of approximately 17 log quanta cm^{-2} s^{-1}.

dark-adapted conditions, the various ipRGC types exhibit diverse spontaneous spike rates spanning an impressively wide range (Fig. 2*C*). This is one of the most salient differences among the five cell types and may facilitate their differentiation in MEA extracellular spike recordings. Specifically, the units that spike spontaneously at over 50 Hz would almost certainly be M4 and/or M5 cells, whereas those with the lowest spontaneous firing rates are probably M1 cells. Importantly, even though M1 cells spike the least in the dark, all M1 cells exhibited spontaneous firing. Given that these cells innervate the SCN (Berson *et al.* 2002; Hattar *et al.* 2006), their spontaneous spiking activity may account for the observation that the eye regulates the circadian pacemaker even in the absence of light (Lee *et al.* 2003).

Melanopsin-based light responses

Earlier investigations using light-adapted retinas reported the intrinsic light responses of M1 cells to be faster, larger and lower threshold than those of M2–M4 cells (Ecker *et al.* 2010; Schmidt & Kofuji, 2011). We have confirmed this finding for dark-adapted ipRGCs and have extended the comparison to include M5 cells. Our observation that all the non-M1 cells had fairly similar amplitude *vs.* intensity relationships (Fig. 3*B* and *C*) is consistent with the report by Tu *et al.* (2005) that MEA recordings of dark-adapted adult mouse ipRGCs showed only two varieties of intrinsic light responses. However, this observation is somewhat surprising, considering that M4 and M5 cells express far less melanopsin than M2 cells (Berson *et al.* 2010; Ecker *et al.* 2010; Estevez *et al.* 2012). Thus, differences in melanopsin expression level do not necessarily correlate with differences in sensitivity or response amplitude, although they could conceivably contribute to differences in kinetics (Fig. 3*D*). An interesting hypothesis is that M4 and M5 cells generate larger single-photon responses than M2 cells, to compensate for their lower melanopsin density (Do *et al.* 2009). However, a caveat is that our *opn4*$^{Cre/+}$*;GFP* ipRGCs contained only one copy of the melanopsin gene, whereas wild-type cells have two copies, and so it is possible that the intrinsic light responses of our ipRGCs differ from those of wild-type cells.

Synaptically driven light responses

Multielectrode array-recorded ipRGCs were previously shown to generate rod-driven light responses (Wong *et al.* 2007; Wong, 2012; Weng *et al.* 2013), although it is unclear whether the ipRGCs sampled in those studies included all five morphological types. We have now obtained the first definitive proof that all five cell types generate rod-mediated light responses, whose threshold intensity of $\sim$7 log quanta cm^{-2} s^{-1} (Fig. 4) are roughly 3–4 log units lower than for epifluorescence-targeted ipRGCs (Fig. 1*D*; Schmidt & Kofuji, 2010; Estevez *et al.* 2012). The rod input to M1 cells, which innervate the master circadian pacemaker (Berson *et al.* 2002; Hattar *et al.* 2006), is consistent with the high sensitivity of SCN neurons to dim light (Aggelopoulos & Meissl, 2000), the low-intensity threshold for circadian photoentrainment (Butler & Silver, 2011) and the ability of rods to drive circadian photoentrainment (Altimus *et al.* 2010). In contrast, neurons in another ipRGC-recipient area, the olivary pretectal nucleus (OPN), have been shown to be insensitive to dim light (Allen *et al.* 2011), and the intensity threshold for pupillary light reflexes (which are driven by the OPN) is nearly 4 log units higher than that for photoentrainment (Butler & Silver, 2011). Thus, it seems plausible that the rod signals carried by ipRGCs are filtered out before they reach the OPN.

For all ipRGC types, full-field illumination evoked sustained extrinsic responses that lasted for the duration of our 10 s stimuli at all intensities (Fig. 4*A*). While the peak amplitudes of these responses varied somewhat among the ipRGC types (Fig. 4*B*, left traces), their kinetics were remarkably uniform across the cell types (Fig. 4*B*, right traces). In contrast, under more light-adapted conditions, M1 cells were previously shown to generate relatively transient and much smaller extrinsic photoresponses than M2 cells (Schmidt & Kofuji, 2009), suggesting that the cone-driven synaptic inputs to ipRGCs may be more diverse than the rod-driven inputs to these ganglion cells. Two possible explanations are that M1 and M2 cells receive input from different types of cone bipolar cells and that the light-adaptive signal dopamine has different effects on M1 *vs.* M2 cells. Dopamine has been shown to modulate rat M1 cells (Van Hook *et al.* 2012), but whether it also impacts M2 has not been investigated.

An electron microscopy study revealed that melanopsin-immunoreactive dendrites are postsynaptic from amacrine cells in the 'off' as well as 'on' sublaminas of the inner plexiform layer (Belenky *et al.* 2003). While the 'on'-channel amacrine input had been confirmed electrophysiologically (Viney *et al.* 2007; Wong *et al.* 2007), the 'off'-channel amacrine input remained elusive until the present study (Fig. 5, arrows). This 'off' input was observed only for M1 and M3 cells, as expected because these are the only ipRGCs with 'off'-sublamina dendrites. We further found that for all ipRGC types, 'on' bipolar-driven light responses are more sustained than 'on' amacrine-driven ones (Fig. 5); thus, during a light step, excitation outlasts inhibition, which can account for the sustained depolarizing light responses observed in current-clamp recordings (Fig. 4*A*). There is immunohistochemical evidence that in the macaque, M1-like cells receive more inhibitory input than M2-like cells (Neumann *et al.* 2011). However, we noticed that amacrine-driven photocurrents tended to be larger in mouse M2 cells than M1 cells (Fig. 5, top traces).

Receptive field properties and potential roles in vision

The receptive fields of M1- and M2-like ipRGCs in primates and of SCN-projecting retinal gangtion cells in cats have been shown to comprise only a centre region (Pu, 2000; Dacey *et al.* 2005). We have found that the receptive fields of mouse M1 cells likewise lack antagonistic surrounds. This observation suggests that these cells probably do not encode spatial contrast, consistent with their primary role in non-image-forming vision (Hattar *et al.* 2006) and with the centre-only receptive fields of SCN neurons (Groos & Mason, 1980). Interestingly, the excitatory and inhibitory synaptic currents of M1 cells show pronounced surround suppression (Fig. 6*B*). The lack of such suppression in the voltage response indicates that the surround effects of the excitatory and inhibitory inputs probably largely cancel out. We further observed that the 'on' amacrine input to M1 cells is spatially more restricted than the 'on' bipolar input (Fig. 6*C*). A plausible explanation is that while 'on' bipolar cells synapse onto the entire dendritic field of an M1 cell, including its distal dendrites in the 'off' sublamina (Wong *et al.* 2007; Dumitrescu *et al.* 2009; Hoshi *et al.* 2009), 'on' amacrine input occurs only on the proximal dendrites of the M1 cell in the 'on' sublamina.

The M4 cells in mice were previously demonstrated to have centre–surround receptive fields (Estevez *et al.* 2012), and we found that the same is true for M2, M3 and M5 cells. As mentioned earlier, the M2-like ipRGCs in the macaque lack centre–surround antagonism (Dacey *et al.* 2005), suggesting that, although these cells resemble mouse M2 cells morphologically, they are not functionally equivalent.

In contrast to an earlier report that SCN-projecting cat RGCs were insensitive to moving lights (Pu, 2000), we have shown that all mouse ipRGCs can respond well to motion speeds up to at least 180 deg s^{-1} (Fig. 7*B*). This ability may be explained by the rapid photoresponses of ipRGCs (Fig. 4*A*); as a moving light appears within the 'on' centre of the receptive field, it induces a robust depolarizing response almost instantly, thus enabling the cell to respond even to a fast-moving stimulus that traverses the 'on' centre only briefly. Even though none of the ipRGCs tested showed any selectivity for the direction of motion, M1–M4 cells responded optimally to different speeds and thus could encode information about this aspect of motion.

The centre–surround receptive fields of M2–M5 cells and the speed tuning properties of M1–M4 ipRGCs suggest that they are suited for spatial and motion analyses. Indeed, M4 cells and ipRGCs with smaller somas (probably M2 and/or M5) have been shown to project to the dLGN, the primary thalamic relay of retinal information to the cortex (Estevez *et al.* 2012). An anatomical study demonstrated a modest projection of M1 cells to the SC (Hattar *et al.* 2006), which integrates sensory and motor information to direct head and eye movements towards novel stimuli, and which also provides an alternative pathway to the visual cortex. We have confirmed this M1 projection and further shown that M2–M4 cells also innervate the SC, although we cannot definitively rule out a retinotectal projection by M5 cells, considering the rarity of this cell type. The different speed preferences of M1–M4 cells may contribute to the diverse speed response profiles of motion-sensitive SC neurons (Waleszczyk *et al.* 1999; Wang *et al.* 2001). Superior colliculus neurons that prefer high speeds have been reported to be highly spontaneously active and to be driven mainly by Y-type retinal ganglion cells (Wang *et al.* 2001); these ganglion cells probably include M4 cells, because this ipRGC type spikes spontaneously at high rates (Fig. 2*C*), responds best to relatively high motion speeds (Fig. 7*B*) and generates Y-cell-like photoresponses (Estevez *et al.* 2012).

The non-M1-type ipRGCs also project to the OPN (Baver *et al.* 2008; Ecker *et al.* 2010), a non-image-forming visual nucleus. The receptive fields of tonic 'on' neurons in the rat OPN have large surrounds (Trejo & Cicerone, 1984), which presumably reflect the surrounds detected in the non-M1 ipRGCs. The functional relevance of centre–surround interaction to the pupillary reflex remains unknown. Interestingly, OPN cells in primates do not show any obvious surround inhibition (Clarke *et al.* 2003), consistent with the lack of such inhibition in the receptive fields of primate ipRGCs (Dacey *et al.* 2005).

References

Aggelopoulos NC & Meissl H (2000). Responses of neurones of the rat suprachiasmatic nucleus to retinal illumination under photopic and scotopic conditions. *J Physiol* **523**, 211–222.

Allen AE, Brown TM & Lucas RJ (2011). A distinct contribution of short-wavelength-sensitive cones to light-evoked activity in the mouse pretectal olivary nucleus. *J Neurosci* **31**, 16833–16843.

Altimus CM, Güler AD, Alam NM, Arman AC, Prusky GT, Sampath AP & Hattar S (2010). Rod photoreceptors drive circadian photoentrainment across a wide range of light intensities. *Nat Neurosci* **13**, 1107–1112.

Barlow HB, Hill RM & Levick WR (1964). Retinal Ganglion cells responding selectively to direction and speed of image motion in the rabbit. *J Physiol* **173**, 377–407.

Baver SB, Pickard GE & Sollars PJ (2008). Two types of melanopsin retinal ganglion cell differentially innervate the hypothalamic suprachiasmatic nucleus and the olivary pretectal nucleus. *Eur J Neurosci* **27**, 1763–1770.

Belenky MA, Smeraski CA, Provencio I, Sollars PJ & Pickard GE (2003). Melanopsin retinal ganglion cells receive bipolar and amacrine cell synapses. *J Comp Neurol* **460**, 380–393.

Berson DM, Castrucci AM & Provencio I (2010). Morphology and mosaics of melanopsin-expressing retinal ganglion cell types in mice. *J Comp Neurol* **518**, 2405–2422.

Berson DM, Dunn FA & Takao M (2002). Phototransduction by retinal ganglion cells that set the circadian clock. *Science* **295**, 1070–1073.

Brainard DH (1997). The Psychophysics Toolbox. *Spat Vis* **10**, 433–436.

Brown TM, Gias C, Hatori M, Keding SR, Semo M, Coffey PJ, Gigg J, Piggins HD, Panda S & Lucas RJ (2010). Melanopsin contributions to irradiance coding in the thalamo-cortical visual system. *PLoS Biol* **8**, e1000558.

Brown TM, Tsujimura S, Allen AE, Wynne J, Bedford R, Vickery G, Vugler A & Lucas RJ (2012). Melanopsin-based brightness discrimination in mice and humans. *Curr Biol* **22**, 1134–1141.

Butler MP & Silver R (2011). Divergent photic thresholds in the non-image-forming visual system: entrainment, masking and pupillary light reflex. *Proc Biol Sci* **278**, 745–750.

Calvert PD, Krasnoperova NV, Lyubarsky AL, Isayama T, Nicoló M, Kosaras B, Wong G, Gannon KS, Margolskee RF, Sidman RL, Pugh EN Jr, Makino CL & Lem J (2000). Phototransduction in transgenic mice after targeted deletion of the rod transducin α-subunit. *Proc Natl Acad Sci U S A* **97**, 13913–13918.

Chang B, Dacey MS, Hawes NL, Hitchcock PF, Milam AH, Atmaca-Sonmez P, Nusinowitz S & Heckenlively JR (2006). Cone photoreceptor function loss-3, a novel mouse model of achromatopsia due to a mutation in *Gnat2*. *Invest Ophthalmol Vis Sci* **47**, 5017–5021.

Clarke RJ, Zhang H & Gamlin PD (2003). Primate pupillary light reflex: receptive field characteristics of pretectal luminance neurons. *J Neurophysiol* **89**, 3168–3178.

Cohen HI, Winters RW & Hamasaki DI (1980). Response of X and Y cat retinal ganglion cells to moving stimuli. *Exp Brain Res* **38**, 299–303.

Dacey DM, Liao HW, Peterson BB, Robinson FR, Smith VC, Pokorny J, Yau KW & Gamlin PD (2005). Melanopsin-expressing ganglion cells in primate retina signal colour and irradiance and project to the LGN. *Nature* **433**, 749–754.

Do MT, Kang SH, Xue T, Zhong H, Liao HW, Bergles DE & Yau KW (2009). Photon capture and signalling by melanopsin retinal ganglion cells. *Nature* **457**, 281–287.

Dumitrescu ON, Pucci FG, Wong KY & Berson DM (2009). Ectopic retinal ON bipolar cell synapses in the OFF inner plexiform layer: contacts with dopaminergic amacrine cells and melanopsin ganglion cells. *J Comp Neurol* **517**, 226–244.

Ecker JL, Dumitrescu ON, Wong KY, Alam NM, Chen SK, LeGates T, Renna JM, Prusky GT, Berson DM & Hattar S (2010). Melanopsin-expressing retinal ganglion-cell photoreceptors: cellular diversity and role in pattern vision. *Neuron* **67**, 49–60.

Einevoll GT & Plesser HE (2005). Response of the difference-of-Gaussians model to circular drifting-grating patches. *Vis Neurosci* **22**, 437–446.

Estevez ME, Fogerson PM, Ilardi MC, Borghuis BG, Chan E, Weng S, Auferkorte ON, Demb JB & Berson DM (2012). Form and function of the M4 cell, an intrinsically photosensitive retinal ganglion cell type contributing to geniculocortical vision. *J Neurosci* **32**, 13608–13620.

Euler T, Hausselt SE, Margolis DJ, Breuninger T, Castell X, Detwiler PB & Denk W (2009). Eyecup scope—optical recordings of light stimulus-evoked fluorescence signals in the retina. *Pflugers Arch* **457**, 1393–1414.

Frechette ES, Sher A, Grivich MI, Petrusca D, Litke AM & Chichilnisky EJ (2005). Fidelity of the ensemble code for visual motion in primate retina. *J Neurophysiol* **94**, 119–135.

Galindo-Romero C, Jiménez-López M, García-Ayuso D, Salinas-Navarro M, Nadal-Nicolás FM, Agudo-Barriuso M, Villegas-Pérez MP, Avilés-Trigueros M & Vidal-Sanz M (2013). Number and spatial distribution of intrinsically photosensitive retinal ganglion cells in the adult albino rat. *Exp Eye Res* **108**, 84–93.

Groos GA & Mason R (1980). The visual properties of rat and cat suprachiasmatic neurones. *J Comp Physiol* **135**, 349–356.

Hattar S, Kumar M, Park A, Tong P, Tung J, Yau KW & Berson DM (2006). Central projections of melanopsin-expressing retinal ganglion cells in the mouse. *J Comp Neurol* **497**, 326–349.

Hattar S, Lucas RJ, Mrosovsky N, Thompson S, Douglas RH, Hankins MW, Lem J, Biel M, Hofmann F, Foster RG & Yau KW (2003). Melanopsin and rod–cone photoreceptive systems account for all major accessory visual functions in mice. *Nature* **424**, 76–81.

Hoshi H, Liu WL, Massey SC & Mills SL (2009). ON inputs to the OFF layer: bipolar cells that break the stratification rules of the retina. *J Neurosci* **29**, 8875–8883.

Hu C, Hill DD & Wong KY (2013). Intrinsic physiological properties of the five types of mouse ganglion-cell photoreceptors. *J Neurophysiol* **109**, 1876–1889.

Lee BB & Willshaw DJ (1978). Responses of the various types of cat retinal ganglion cells to moving contours. *Vision Res* **18**, 757–765.

Lee HS, Nelms JL, Nguyen M, Silver R & Lehman MN (2003). The eye is necessary for a circadian rhythm in the suprachiasmatic nucleus. *Nat Neurosci* **6**, 111–112.

Lucas RJ, Hattar S, Takao M, Berson DM, Foster RG & Yau KW (2003). Diminished pupillary light reflex at high irradiances in melanopsin-knockout mice. *Science* **299**, 245–247.

Neumann S, Haverkamp S & Auferkorte ON (2011). Intrinsically photosensitive ganglion cells of the primate retina express distinct combinations of inhibitory neurotransmitter receptors. *Neuroscience* **199**, 24–31.

Pu M (2000). Physiological response properties of cat retinal ganglion cells projecting to suprachiasmatic nucleus. *J Biol Rhythms* **15**, 31–36.

Rodieck RW (1965). Quantitative analysis of cat retinal ganglion cell response to visual stimuli. *Vision Res* **5**, 583–601.

Schmidt TM & Kofuji P (2009). Functional and morphological differences among intrinsically photosensitive retinal ganglion cells. *J Neurosci* **29**, 476–482.

Schmidt TM & Kofuji P (2010). Differential cone pathway influence on intrinsically photosensitive retinal ganglion cell subtypes. *J Neurosci* **30**, 16262–16271.

Schmidt TM & Kofuji P (2011). Structure and function of bistratified intrinsically photosensitive retinal ganglion cells in the mouse. *J Comp Neurol* **519**, 1492–1504.

Schmidt TM, Taniguchi K & Kofuji P (2008). Intrinsic and extrinsic light responses in melanopsin-expressing ganglion cells during mouse development. *J Neurophysiol* **100**, 371–384.

Sexton TJ, Golczak M, Palczewski K & Van Gelder RN (2012). Melanopsin is highly resistant to light and chemical bleaching *in vivo*. *J Biol Chem* **287**, 20888–20897.

Trejo LJ & Cicerone CM (1984). Cells in the pretectal olivary nucleus are in the pathway for the direct light reflex of the pupil in the rat. *Brain Res* **300**, 49–62.

Tu DC, Zhang D, Demas J, Slutsky EB, Provencio I, Holy TE & Van Gelder RN (2005). Physiologic diversity and development of intrinsically photosensitive retinal ganglion cells. *Neuron* **48**, 987–999.

Van Hook MJ, Wong KY & Berson DM (2012). Dopaminergic modulation of ganglion-cell photoreceptors in rat. *Eur J Neurosci* **35**, 507–518.

Viney TJ, Balint K, Hillier D, Siegert S, Boldogkoi Z, Enquist LW, Meister M, Cepko CL & Roska B (2007). Local retinal circuits of melanopsin-containing ganglion cells identified by transsynaptic viral tracing. *Curr Biol* **17**, 981–988.

Waleszczyk WJ, Wang C, Burke W & Dreher B (1999). Velocity response profiles of collicular neurons: parallel and convergent visual information channels. *Neuroscience* **93**, 1063–1076.

Wang C, Waleszczyk WJ, Benedek G, Burke W & Dreher B (2001). Convergence of Y and non-Y channels onto single neurons in the superior colliculi of the cat. *Neuroreport* **12**, 2927–2933.

Warren EJ, Allen CN, Brown RL & Robinson DW (2003). Intrinsic light responses of retinal ganglion cells projecting to the circadian system. *Eur J Neurosci* **17**, 1727–1735.

Wei W, Elstrott J & Feller MB (2010). Two-photon targeted recording of GFP-expressing neurons for light responses and live-cell imaging in the mouse retina. *Nat Protoc* **5**, 1347–1352.

Weng S, Estevez ME & Berson DM (2013). Mouse ganglion-cell photoreceptors are driven by the most sensitive rod pathway and by both types of cones. *PLoS One* **8**, e66480.

Wong KY (2012). A retinal ganglion cell that can signal irradiance continuously for 10 hours. *J Neurosci* **32**, 11478–11485.

Wong KY, Dunn FA & Berson DM (2005). Photoreceptor adaptation in intrinsically photosensitive retinal ganglion cells. *Neuron* **48**, 1001–1010.

Wong KY, Dunn FA, Graham DM & Berson DM (2007). Synaptic influences on rat ganglion-cell photoreceptors. *J Physiol* **582**, 279–296.

Additional Information

Competing interests

None declared.

Author contributions

X.Z. performed all electrophysiological recordings, contributed to the experimental design, performed the SC injections and analysed all electrophysiological data; B.K.S. supervised the SC injections, imaged the injection sites, analysed the difference-of-Gaussians data and edited the manuscript; A.L.G. and W.M.K. provided technical help and equipment for the SC injections; K.Y.W. conceived the project, designed the research, supervised his team members, interpreted the data and drafted and revised the manuscript. The SC injections were performed in W.M.K.'s laboratory, whereas all the other experiments were performed in K.Y.W.'s laboratory. All authors reviewed and approved the final version of the manuscript.

Funding

This work was funded by National Eye Institute (NEI) Grants R00 EY018863 and R01 EY023660 to K.Y.W., a Research to Prevent Blindness Scientific Career Development Award to K.Y.W., NEI Grant F32 EY021063 to B.K.S., and NEI Grant P30 EY007003 to the Kellogg Eye Center.

Acknowledgements

We thank Samer Hattar for providing breeding stocks of *opn4*^{Cre} mice for creating *opn4*$^{Cre/+}$;*GFP* mice, and Janis Lem and Bo Chang for providing breeding stocks of *Gnat1*$^{-/-}$ and *Gnat2*^{cpfl3} mice.